Antidepressants promote developmental-like plasticity through remodeling of extracellular matrix

Phi T. Nguyen[1,2], Shogo Tamura[1], Emily Sun[1,2], Yuecheng Shi[1,2], Yang Xiao[3,4], Clay Lacefield[1,2], Gergely Turi[1,2], René Hen[1,2]

Affiliations:
[1] *Department of Psychiatry, Columbia University Irving Medical Center, New York, NY 10032, USA*
[2] *Division of Systems Neuroscience, New York State Psychiatric Institute, New York, NY 10032, USA*
[3] *Department of Biomedical Engineering, Columbia University, New York, NY 10027, USA*
[4] *Department of Systems Biology, Columbia University Irving Medical Center, New York, NY 10032, USA*

Abstract
Selective serotonin reuptake inhibitors like Fluoxetine (Flx) are widely used to treat mood and anxiety disorders. Despite decades of use, the molecular logic by which they modulate stress-related behaviors remain poorly understood. Here we show that Flx reactivates a developmental-like plasticity program in the dentate gyrus (DG) by remodeling the extracellular matrix (ECM). Single-nucleus RNA sequencing of the hippocampus post-Flx revealed robust transcriptomic reprogramming in the DG, with mature granule cells adopting a juvenile-like transcriptional profile, including upregulation of the developmental gene *Sox11*. This was accompanied by increased BDNF signaling and enhanced structural remodeling in the mossy fiber pathway. Flx remodeled perisynaptic nets, a novel ECM structures in the DG, and targeted ECM degradation around granule cells reactivated SOX11. Flx treatment mitigated stress-induced fear generalization, and this was phenocopied by direct degradation of ECM in the DG. These findings identify ECM remodeling as a molecular substrate for Flx's effects, linking induction of a developmental-like plasticity program and rejuvenation of mature granule cells to improvements in stress-induced overgeneralization.

Introduction
Mood and anxiety disorders, such as major depressive disorder (MDD), are among the most prevalent forms of mental illness and are a leading cause of disability worldwide (1). Although selective serotonin reuptake inhibitors (SSRIs) have been widely used as first-line treatments for decades, they achieve remission in only about one-third of patients. This limited efficacy underscores the urgent need to elucidate the cell and molecular mechanisms underlying antidepressant effects.

Imaging and post-mortem studies have implicated the hippocampus with MDD and other mood disorders (2). The hippocampus is particularly vulnerable to chronic stress, a common risk factor for mood and anxiety disorders. Chronic stress disrupts hippocampal function and induces structural deficits, including reduced dendritic spine density. Within the hippocampus, the dentate gyrus (DG) has been identified as a critical region for mediating the behavioral effects of SSRIs like fluoxetine (Flx). The DG comprises a heterogeneous population of granule cells, including mature neurons and a subset of newborn neurons generated through adult neurogenesis. Both mature and immature granule cells have been shown to be essential for the behavioral effects of chronic Flx in rodent models (3,4). While bulk transcriptomic studies have identified molecular regulators such as *Bdnf* that could contribute to SSRI efficacy, the functional roles of these regulators in specific granule cell subsets remain poorly understood.

In this study, we found that mature granule cells in the DG exhibit a selective transcriptional response to Flx, characterized by the reactivation of a developmental-like plasticity program. This response is time-dependent, emerging only after 3 weeks of Flx treatment, consistent with the delayed therapeutic effects of SSRIs in patients. Moreover, we show that Flx remodels perisynaptic nets, a novel extracellular matrix (ECM) structure in the DG, and direct degradation of ECM mitigated stress-induced overgeneralization. These findings highlight ECM remodeling as a critical mechanism underlying Flx-induced plasticity and identify mature granule cells as key mediators of its effects on behavior.

Results

Fluoxetine mitigates stress-induced fear generalization in a mouse model

To investigate the cellular mechanisms by which SSRIs modulate stress-induced behaviors, we used an established mouse model of chronic stress and Fluoxetine treatment (**Fig. 1A**). Elevated glucocorticoid levels are a common feature in various mood disorders (5). Accordingly, chronic treatment with the glucocorticoid corticosterone (Cort) in rodents induces stress-related behavioral impairments (6). Mice were exposed to Cort for 3 weeks before a subgroup received either short-term (5 days) or long-term (3 weeks) fluoxetine (Flx) treatment. In the elevated plus maze (EPM), Cort-treated mice showed reduced exploration of the anxiogenic open arm, which was reversed by 3 weeks of Flx (**Fig. 1B**, and **Fig. S1A**). However, no difference was observed after 5 days of Flx, mirroring the delayed onset of SSRI effects in patients. Similarly, in the novelty suppressed feeding (NSF) test a test of innate anxiety, Cort-treated mice exhibited an increased latency to feed in the anxiogenic arena that was rescued by 3 weeks of Flx treatment, but not 5 days (**Fig. 1C**, and **Fig. S1B**).

Mood and stress disorders are characterized by cognitive deficits, including learning and memory impairments and a bias towards remembering negative information (7). In addition to measuring innate anxiety, we used a contextual fear generalization task to examine stress-induced memory and negativity bias overtime. Mice were fear conditioned to an arena with a 2s footshock (context A) over the course of three days and then exposed to the conditioned context followed by an unconditioned arena with similar contextual features (context B; **Fig. 1D**). We then measured their ability to discriminate between the two contexts at 1 and 14 days post-training by measuring their freezing levels (**Fig. 1E-F**, and **Fig. S1C**). Mice in the Vehicle group showed normal memory recall and the ability to differentiate between contexts A and B, although this ability declined by day 14, reflecting memory generalization overtime. Cort-treated mice could discriminate on day 1, but this ability was completely abolished by day 14. This stress-induced increase in fear memory generalization was reversed after 3 weeks of Flx treatment and these effects were consistent across sexes (**Fig. S1D**). Interestingly, the Cort group showed an overall increase in freezing behavior, which was also reversed by Flx treatment. In summary, our data establish a mouse model for investigating the cellular substrates through which Flx modulates stress-induced emotional memory function.

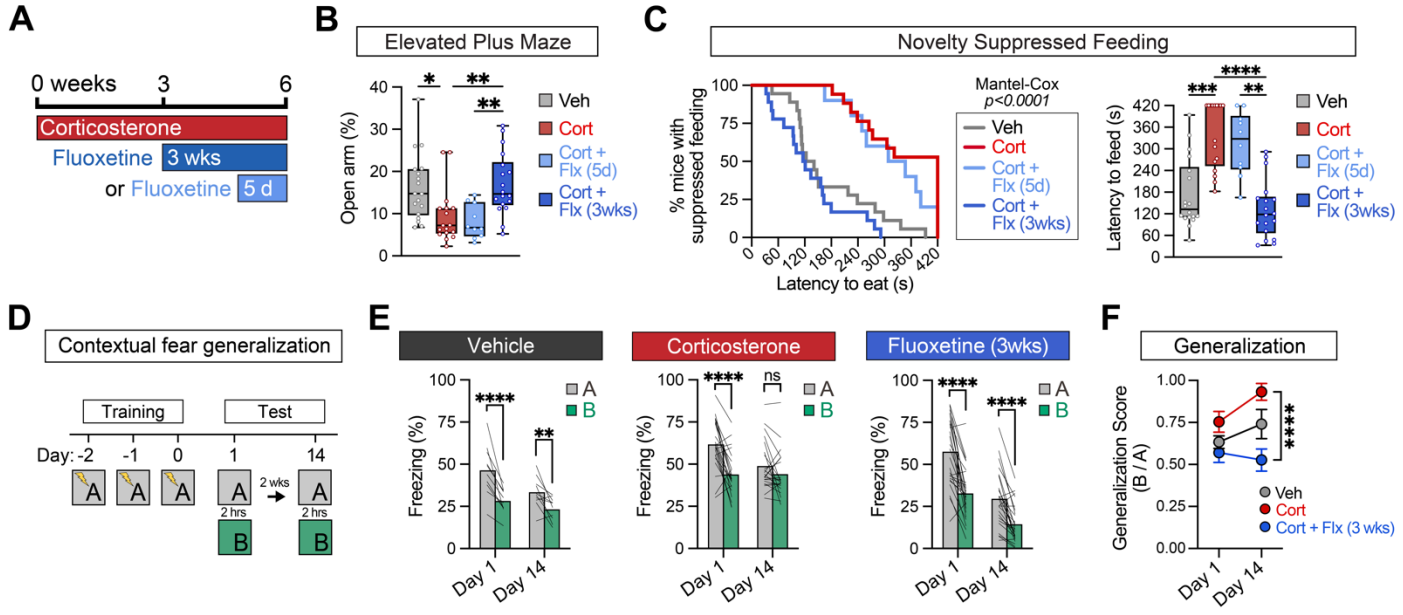

Figure 1. Fluoxetine mitigates stress-induced anxiety and fear generalization. (**A**) Pharmacological approach. Corticosterone (35 ug/mL) and Fluoxetine (160 ug/mL) were delivered in drinking water. (**B**) Time spent in the open arm of the EPM per mouse (One-way ANOVA, Tukey's multiple comparisons test, n=18 (Veh), 17 (Cort), 10 (Flx 5d), 18 (Flx 3wks)). (**C**) Latency to feed in NSF per mouse shown as survival curve (left; Log-rank Mantel-Cox test, $\chi 2=39.21$, $p<0.0001$) and box plot (right; Kruskal-Wallis test, Dunn's multiple comparisons test), n= same as (B)). (**D**) Schematic of contextual fear generalization assay. (**E**) Freezing in the fear conditioned context A versus unconditioned context B at 1 and 14 days post-training for Veh, Cort, and Cort + Flx (3wks) groups (Two-way repeated measures ANOVA, Sidak's post hoc tests, n=10 (Veh), 22 (Cort), 25 (Flx 3wks)). Lines connect paired data for each mouse. (**F**) Generalization scores at 1 and 14 days calculated as the freezing time in context B divided by context A (Two-way repeated measures ANOVA, Tukey's multiple comparisons tests). Data = mean ± SD. *$p < 0.05$; **$p < 0.01$; ***$p < 0.001$; ****$p < 0.0001$.

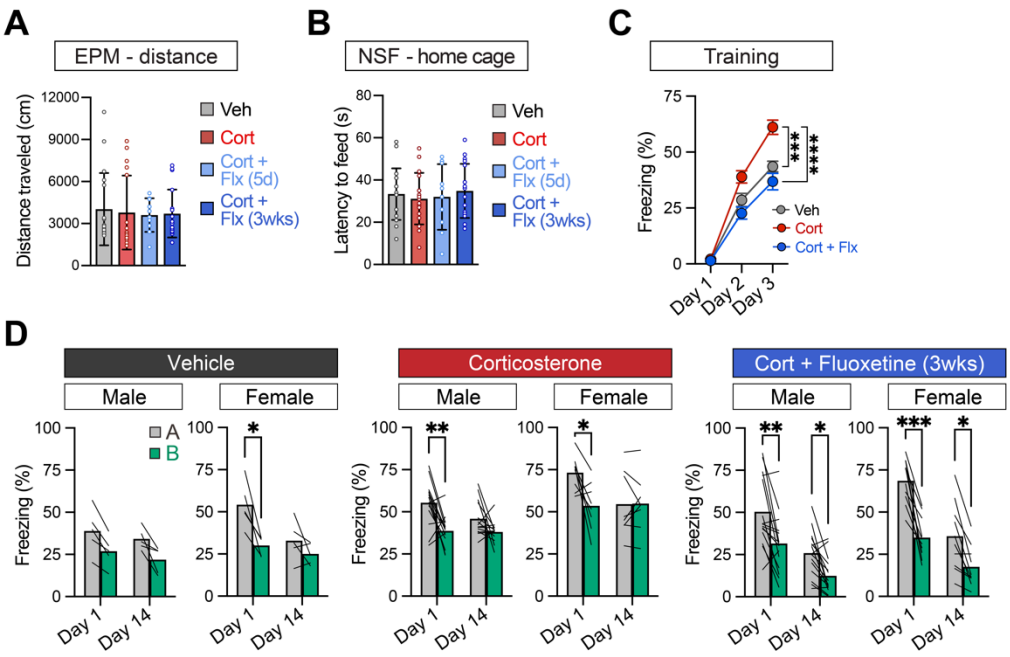

Supplementary Figure 1. (**A**) Distance traveled in the EPM per mouse (One-way ANOVA, p= 0.96, n=18 (Veh), 17 (Cort), 10 (Flx 5d), 18 (Flx 3wks)). (**B**) Latency to feed in home cage per mouse (One-way ANOVA, p= 0.85, n= same as (A)). (**C**) Freezing levels during contextual fear conditioning (Two-way RM ANOVA, day x condition p< 0.0001, Tukey's post-hoc tests, n=10 (Veh), 22 (Cort), 25 (Flx 3wks)). (**D**) Freezing in context A versus B at 1 and 14 days post-training by sex for each group (Two-way RM ANOVA, Sidak's post-hoc tests, n=5 (Veh-Male), 5 (Veh-Female), 14 (Cort-Male), 8 (Cort-Female), 15 (Flx-Male), 10 (Flx-Female)). Lines connect paired data for each mouse. *$p < 0.05$; **$p < 0.01$; ***$p < 0.001$; ****$p < 0.0001$.

Time-dependent transcriptomic reprogramming in dentate granule cells after fluoxetine treatment

The hippocampus is a critical structure for the precise recall of emotional memories and is highly vulnerable to chronic stress, a common risk factor among mood and anxiety disorders (5,8). To molecularly define the hippocampal substrates underlying antidepressant-like effects post-Flx, we performed droplet-based single nucleus RNA-sequencing (snRNA-seq) of hippocampal cells in mice treated with Cort alone or Cort + Flx at 2 different time points (5 days or 3 weeks, **Fig. 2A**). Five days of Flx treatment was chosen to determine the early events that precede behavioral modulation (**Fig. 1B-C**). We recovered 119, 346 nuclei across all conditions and identified all major neuronal and glial subtypes in the hippocampus for downstream analyses (**Fig. 2B-C**, and **Fig. S1A-D**).

Unsupervised clustering analysis revealed a distinct transcriptomic shift between Cort and Cort + Flx (3wks) groups, which primarily mapped onto DG granule cells and was not present after 5 days of Flx (**Fig. 2D-E**). To quantify the level of transcriptomic reprogramming post-Flx, we measured the number of differentially expressed genes (DEGs) between Cort alone and Cort + Flx groups for each cell type (**Fig. 2F**). All cell types were downsampled to comprise equal number of nuclei for this analysis (588 nuclei per cell type, see *Methods*). After 5 days of Flx treatment, with the exception of microglia, we found little transcriptional activity overall. This was consistent with the lack of behavioral modulation by Flx at this timepoint **Fig. 1B-C**) and raises the possibility that microglia could play a causal role in the Flx response. Whereas a glia response dominated after 5 days of Flx treatment, neuronal responses were more prominent after 3 weeks. Consistent with the transcriptomic shift observed in our unsupervised clustering analysis, DG granule cells had the largest number of differentially expressed genes after 3 weeks of Flx, an effect that was at least ~4-fold greater than any other neuronal cell type. Altogether, these results suggest that granule cells in the DG are highly sensitive to the effects of chronic Flx.

The DG contains a heterogeneous population of granule cells comprised of mature neurons and a subset of newborn neurons generated from adult neurogenesis (9). Both mature and immature granule cells are required for the antidepressant-like effects of chronic Flx in rodent models (3,4). However, little is known

about how these populations drive behavioral modulation. To better understand the heterogeneous responses to Flx, we leveraged the single cell resolution of our approach and subclustered the granule cell population, revealing 3 additional clusters (**Fig. 2G**). Clusters 1 and 2 were identified as mature granule cells, characterized by expression of the mature granule cell marker *Dock10* and absence of the immature granule cell marker *Igfbpl1* (10). Cluster 3 corresponded to immature granule cells (*Igfbpl1*+; **Fig. 2H**). Mature granule cells primarily overlapped with cluster 2 in both Cort alone and Cort + Flx (5d) groups, suggesting minimal transcriptional responses at this timepoint (**Fig. 2I-J**). However, mature granule cells in the Cort + Flx (3 wks) group primarily overlapped with cluster 1, indicating a significant shift towards a distinct cellular state. Immature granule cells maintained a stable cellular state across all conditions but expanded ~4-fold after 3 weeks of Flx, consistent with previous findings that SSRIs can increase hippocampal neurogenesis (11). Overall, we found that differential gene expression changes in granule cells were primarily driven by mature neurons, which accounted for 85.5% of DEGs in the granule cell population after 3 weeks of Flx (**Fig. 2F**). Altogether, these results suggest that Flx induces a time-dependent transcriptomic reprogramming specifically in mature granule cells of the DG.

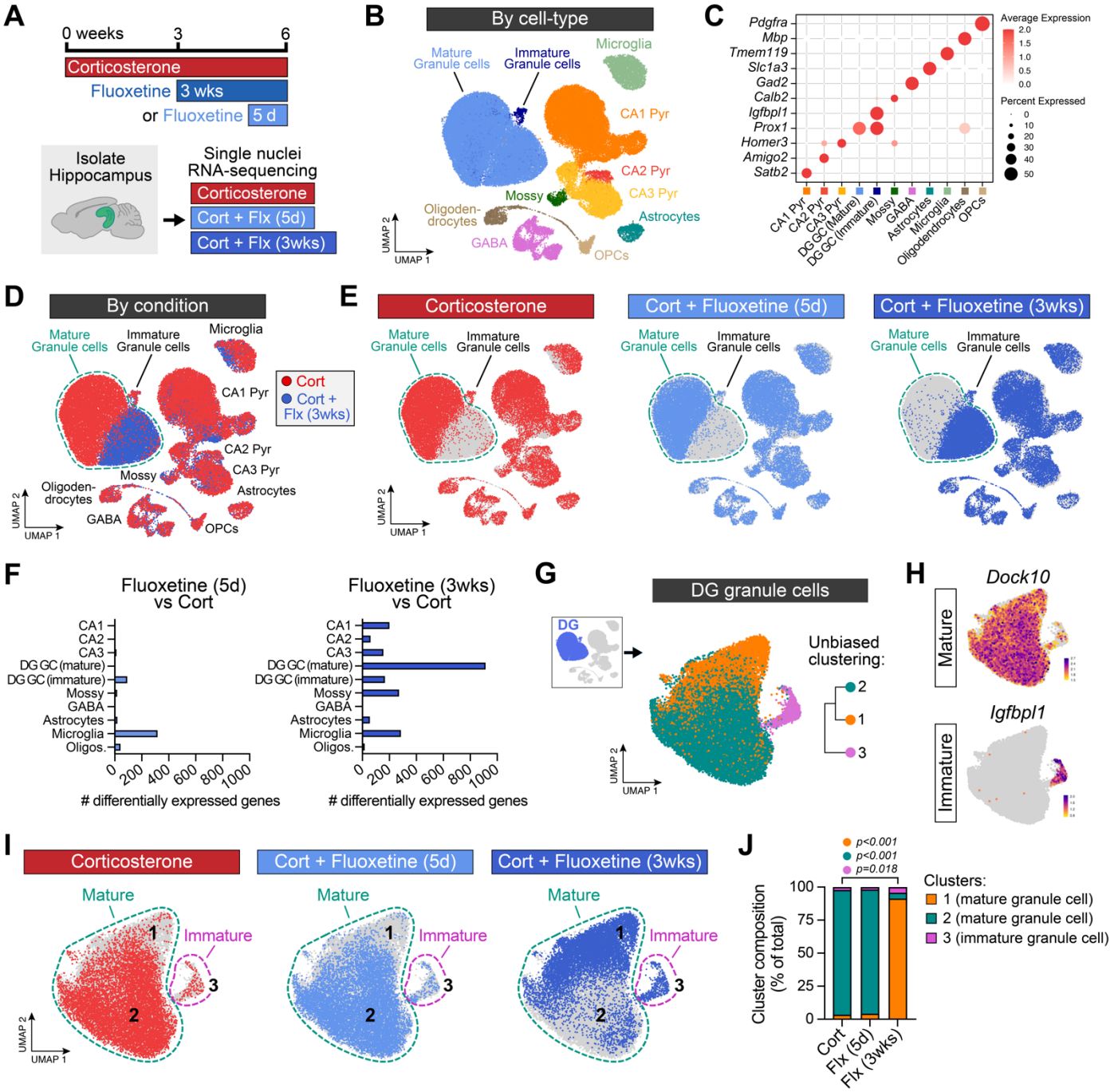

Figure 2. Transcriptomic reprogramming in dentate granule cells after fluoxetine treatment. (**A**) Pharmacological approach for downstream snRNA-seq of hippocampal cells (n=3 mice per condition). (**B**) Unsupervised clustering (uniform manifold approximation and projection (UMAP)) of 119, 346 single nuclei transcriptomic profiles labeled by cell type. (**C**) Expression of cell type-specific marker genes for major neuronal and glial populations. See Fig. S2D for additional marker genes. (**D**) Nuclei from Corticosterone + Fluoxetine (Cort + Flx) group (blue) overlaid with nuclei from Cort alone (red). (**E**) Nuclei highlighted by condition. (**F**) Number of differentially expressed genes (DEGs) between Cort and Cort + Flx groups for each cell type. Each cell type was downsampled to 588 nuclei for all analyses. (**G**) Subclustering of dentate granule cells from (B). (**H**) Expression of maturation-related marker genes in granule cells. (**I**) Granule cell nuclei highlighted by condition. (**J**) Quantification of granule cell cluster composition from (G) by treatment condition (n=3 mice per condition).

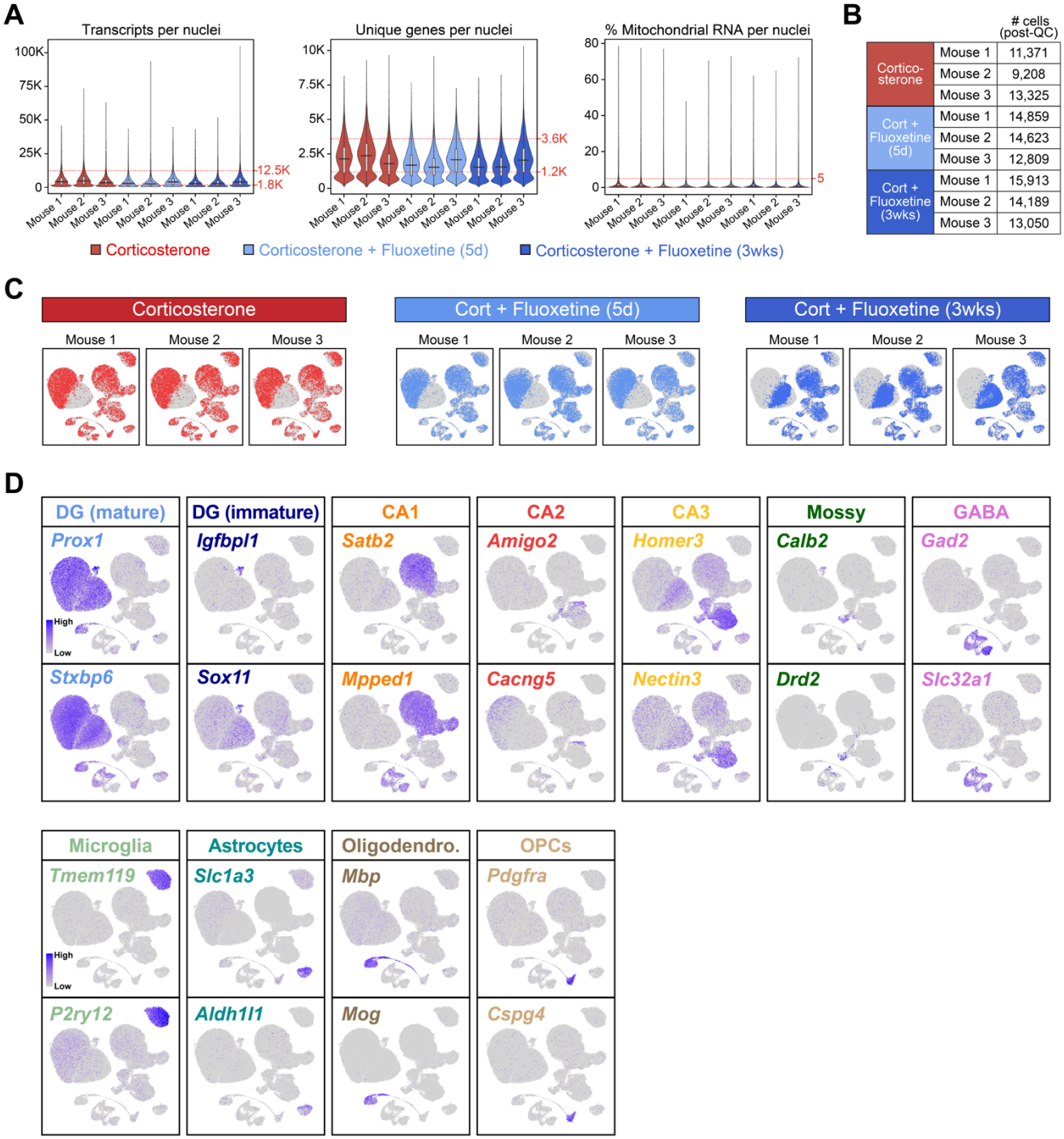

Supplementary Figure 2. (**A**) Quality control metrics for single nuclei RNA-sequencing in Cort, Cort + Flx (5d), and Cort + Flx (3wks) groups. Dashed lines indicate minimum and maximum threshold settings. (**B**) Table showing number of nuclei per mouse per condition after quality control thresholding. (**C**) Comparison of biological replicates following unsupervised clustering of hippocampal nuclei. (**D**) Representative markers for each major neuronal and glia cell type in the hippocampus.

Fluoxetine reactivates a developmental-like plasticity program

Dentate granule cells are essential for Flx's behavioral effects in rodents (3,4), yet the molecular substrates driving these effects remain poorly understood. To investigate this, we ranked DEGs between Cort and Cort + Flx (3 wks) groups, focusing on unique responses in mature granule cells (**Fig. 3A**). In Flx-treated mice, mature granule cells upregulated genes associated with synaptic transmission and remodeling (**Fig. 3B**), including many presynaptic machinery genes (*Nrxn3*, *Sv2c*, and *Syn3*) and downregulation of negative regulators of mossy fiber synaptogenesis (*Sema5a*, *Ablim3*, and *Pten*; (12–14)). Consistent with bulk transcriptomic approaches (15,16), we found increased expression of genes related to neurotrophic signaling (*Bdnf*, *Ntrk2*, and *Acvr1*). Gene ontology analysis revealed novel Flx-driven pathways in mature granule cells, including Developmental Biology (*Sox11*, *Bdnf*, *Nfix*, and *Sema3e*) and Extracellular Matrix Organization (*Adamts6*, *Ptprn*, and *Large1*; **Fig. 3A-B**).

Critical periods are developmental windows of heightened experience-dependent refinement of neural circuits that typically close during late adolescence (17). In adult mice, Flx can reactivate forms of plasticity associated with developmental critical periods, such as ocular dominance plasticity and enhanced axon regeneration (18–21). To assess if Flx activates a latent neurodevelopmental program, we analyzed a scRNA-seq dataset of dentate gyrus development (22), comparing DEGs in juvenile (P5) vs adult (P132) granule cells to generate a juvenile granule cell score from the top 100 upregulated genes (**Fig. 3C**, and **Fig. S3A-B**). As expected, immature granule cells in our dataset closely resembled juvenile granule cells (**Fig. 3D-E**), consistent with findings that adult neurogenesis recapitulates features of neurodevelopment (23). In mature granule cells from our dataset, we found an increased juvenile granule cell score in the Cort + Flx (3 wks) group, which was not present after 5 days of Flx (**Fig. 3D-E**). Mature granule cells in the Cort + Flx (3 wks) group also showed greater similarity to immature granule cells from adult hippocampal neurogenesis and regenerating spinal cord neurons, both of which are associated with an embryonic-like transcriptional state (23–26). The increased resemblance of mature granule cells to a developmental-like state was confirmed in an independent snRNA-seq dataset of hippocampal neurons following treatment with Flx or electroconvulsive shock (ECS; **Fig. S3F-H**). These data suggest that Flx can activate a latent developmental-like transcriptional program.

We next assessed how reactivation of this developmental program could impact dentate function. *Sox11* is a transcription factor critical for maintaining an immature cell state (24,27,28) and is a top gene distinguishing juvenile from adult granule cells in mice and humans (17,22; **Fig. S3B**). Both *Sox11* and *Bdnf*, a neurotrophin with essential roles in neurodevelopment and synaptic plasticity (30,31), were upregulated in mature granule cells after chronic Flx treatment (**Fig. 3F**, and **Fig. S3G**). SOX11 was expressed in 95.5% of PROX1+ granule cells in juvenile mice, but only 7.6% in adults (**Fig. 3G-H**). Most SOX11+ granule cells in adults corresponded to DCX+ immature neurons arising from adult neurogenesis (**Fig. 3I**, and **Fig. S3J**). After 3 weeks of Flx treatment, 52.9% of mature granule cells (PROX1+ DCX-) reactivated SOX11, an effect not observed after 5 days of treatment (**Fig. 3I-J**). Interestingly, we observed SOX11 reactivation occurred primarily in the outer granule cell layer, which is mainly occupied by embryonically generated neurons, and distinct from the inner granule cell layer where adult neurogenesis occurs (32). Consistent with the developmental pattern of *Sox11* expression, *Bdnf* levels were significantly higher in juvenile granule cells compared to adults, and 3 weeks of Flx treatment also increased *Bdnf* expression in mature granule cells (**Fig. 3K-N**). In the hippocampus, BDNF was highly concentrated in the mossy fiber pathway–the axonal projections of dentate granule cells–where it co-localized with ZNT3+ mossy fiber terminals (**Fig. 3O**). Three weeks of Flx treatment significantly increased mossy fiber BDNF levels (**Fig. 3P-Q**). This was consistent with the observed upregulation of presynaptic machinery genes, including an increase in SV2C+ mossy terminals (**Fig. 3A**, and **Fig. S3K-I**). To determine if reactivating a developmental-like program was linked to structural plasticity, we generated a reporter line with sparse labeling of mossy terminals (*Prox1*$^{creER/+}$;*Rosa26*$^{tdTomato/+}$) and identified the two major terminal types: large mossy terminals and *en passant* varicosities (28; **Fig. 3R**). Chronic Flx treatment increased both the number of mossy terminals and the size of these two bouton subtypes (**Fig. 3S-**

T). Altogether, these data uncover a molecular logic by which Flx reactivates a developmental-like plasticity program in the DG and rejuvenates mature granule cells.

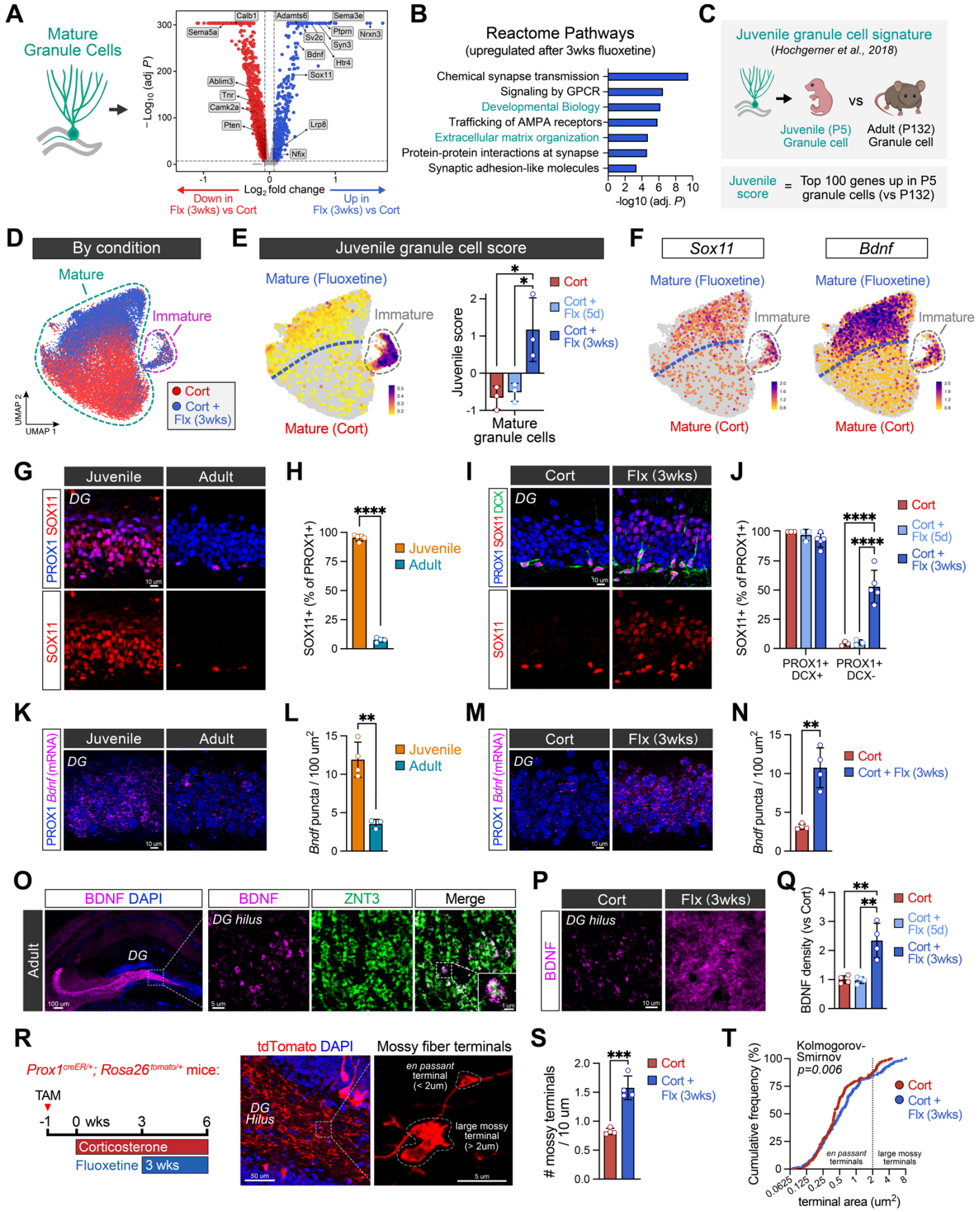

Figure 3. Fluoxetine reactivates a developmental-like plasticity program in mature granule cells. (**A**) Volcano plot of differentially expressed genes between mature granule cells from Cort and Cort + Flx (3wks) groups. (**B**) Top gene ontology terms for upregulated genes in (A). (**C**) Juvenile granule cell score defined as the top 100 genes

upregulated in P5 granule cells versus P132 granule cells. Dataset from (22); also see Fig. S3A-B. (**D**) Transcriptomic profiles of dentate granule cells colored by treatment condition (Cort = red, Cort + Flx (3wks) = blue) and cell type (Mature = green outline, Immature = magenta outline). (**E**) Feature plot showing average expression of juvenile granule cell score (left) and quantification per mouse (right; One-way ANOVA, Tukey's multiple comparisons test, n=3 mice/group). (**F**) Expression of *Sox11* and *Bdnf* in granule cells. (**G**) SOX11 protein expression in the DG of juvenile (P10) and adult (~P120) mice. PROX1 marks granule cell neurons. (**H**) Quantification of SOX11+ granule cells per mouse (t-test, n= 5 (juvenile), 4 (adult)). (**I**) SOX11 protein expression in the DG of adult mice treated with Cort or Cort + Flx (3wks). PROX1 marks granule cells, DCX marks immature granule cells. (**J**) Quantification of SOX11+ in mature (PROX1+ DCX-) and immature (PROX1+ DCX+) granule cells per mouse (One-way ANOVA, Tukey's multiple comparisons test, n=3 (Cort), 3 (Cort + Flx 5d), 5 (Cort + Flx 3wks)). (**K**) *Bdnf* mRNA expression in the DG of juvenile (P10) and adult (~P120) mice. (**L**) Quantification of *Bdnf* mRNA in the DG per mouse (t-test, n= 4 (juvenile), 3 (adult)). (**M**) *Bdnf* mRNA expression in the DG of adult mice treated with Cort or Cort + Flx (3wks). (**N**) Quantification of *Bdnf* mRNA in the DG per mouse (t-test, n= 4 (Cort), 4 (Cort + Flx 3wks)). (**O**) Representative image of BDNF protein expression in the hippocampus. Inset shows higher magnifications of BDNF overlapped with ZNT+ mossy fiber terminals. (**P**) BDNF protein levels in the hilar mossy fiber pathway of adult mice treated with Cort or Cort + Flx (3wks). (**Q**) Quantification of BDNF protein levels in the hilar mossy fiber pathway per mouse (One-way ANOVA, Tukey's multiple comparisons test, n=4 mice/group). (**R**) Schematic for genetic and pharmacological approach to sparsely label mossy fiber terminals (left) and representative images of mossy terminals (right). (**S**) Quantification of mossy fiber terminal numbers per mouse in adult mice treated with Cort or Cort + Flx (3wks) (t-test, n= 4 mice/group). (**T**) Quantification of mossy fiber terminal area as cumulative distribution in adult mice treated with Cort or Cort + Flx (3wks) (Kolmogorov-Smirnov test, n= 200 terminals (Cort), 245 (Cort + Flx 3wks)). Data = mean ± SD. *$p < 0.05$; **$p < 0.01$; ***$p < 0.001$; ****$p < 0.0001$.

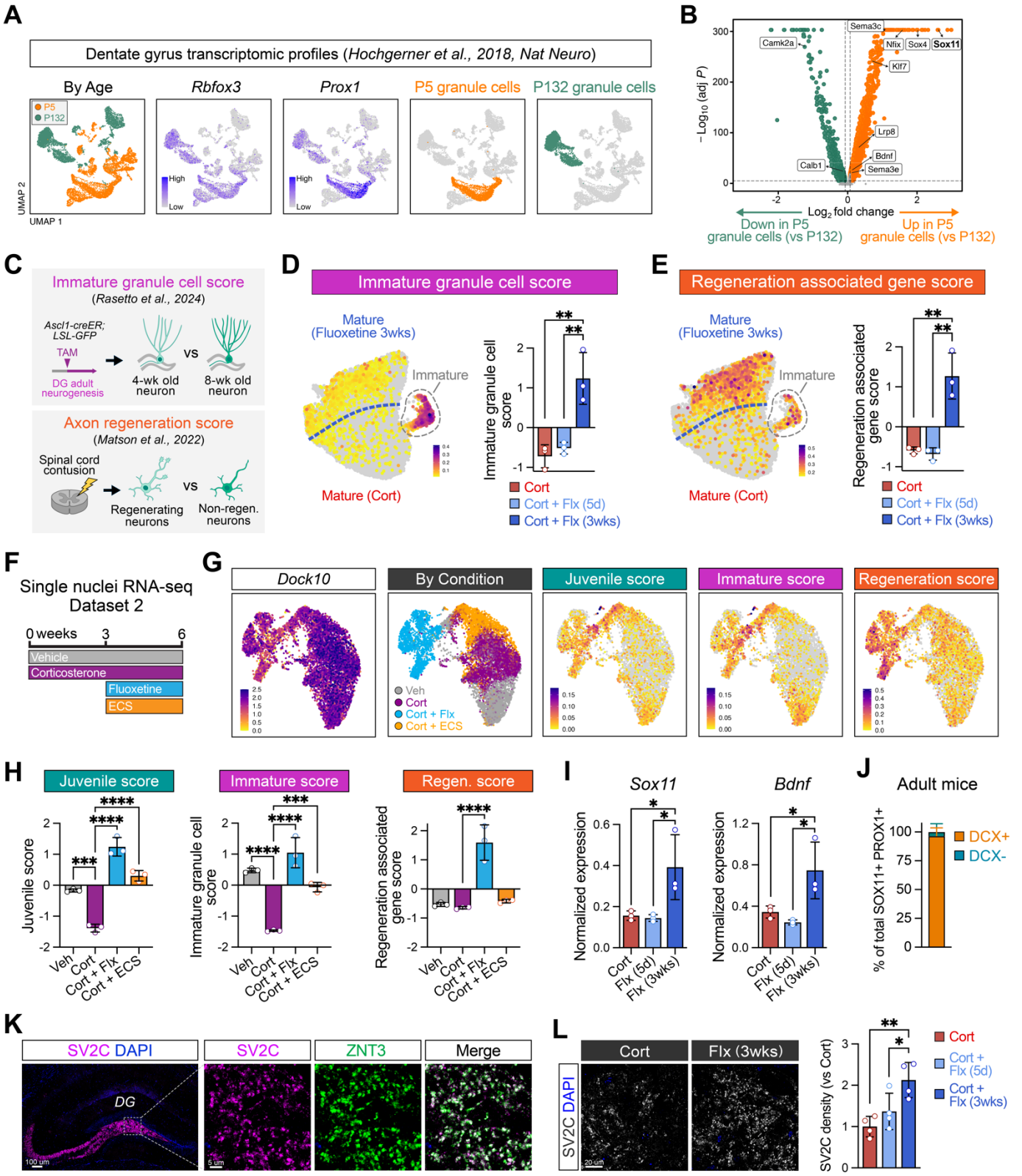

Supplementary Figure 3. (**A**) Analysis of single cell RNA-seq dataset (22) of the dentate gyrus from P5 and P132 mice showing unsupervised clustering analysis and identification of granule cells. (**B**) Volcano plot of differentially expressed genes between P5 versus P132 granule cells from (A). (**C**) Immature granule cell and axon regeneration scores defined as upregulated genes in 4- versus 8-week old neurons generated from adult hippocampal neurogenesis (24) and regenerating versus non-regenerating spinal cord neurons (25). (**D**) Feature plot showing average expression of immature granule cell score (left) and quantification per mouse (right; One-way ANOVA, Tukey's post-hoc test, n=3 mice/group). (**E**) Feature plot showing average expression of regeneration associated gene score (left) and quantification per mouse (right; One-way ANOVA, Tukey's post-hoc test, n=3 mice/group). (**F**)

Schematic for pharmacological and electroconvulsive shock approach for snRNA-seq of hippocampal nuclei (Dataset 2; see *Methods*). (**G**) Unsupervised clustering of dentate granule cells from dataset 2 showing expression of *Dock10* and module scores from Fig. 3C and Fig. S3C. (**H**) Quantification of module scores per mouse from dataset 2 (right; One-way ANOVA, Tukey's post-hoc test, n=3 mice/group). (**I**) Normalized expression of *Sox11* and *Bdnf* in mature granule cells corresponding to Fig. 3F. (**J**) Proportion of DCX+ and DCX- neurons in the SOX11+ PROX1+ granule cell population in adult mice. (**K**) Representative image of SV2C levels in the hippocampus. Inset shows higher magnifications of SV2C overlapped with ZNT+ mossy fiber terminals. (**L**) SV2C protein levels in the hilar mossy fiber pathway of adult mice treated with Cort or Cort + Flx (3wks) and quantification of SV2C density per mouse (One-way ANOVA, Tukey's multiple comparisons test, n=4 mice/group). Data = mean ± SD. *$p < 0.05$; **$p < 0.01$

Turnover of extracellular matrix induces developmental-like plasticity and mitigates stress-induced fear generalization

The extracellular matrix (ECM) is a complex glycoprotein network that stabilizes synapses and restricts plasticity in the mature brain. Perineuronal nets (PNNs), specialized ECM structures encasing neurons, play a key role in closing critical periods towards the end of neurodevelopment (17,34). Removal of PNNs and other ECM structures in adulthood can reactivate critical period-like plasticity, similar to the effects of chronic Flx (35–37). While ECM proteins are highly stable in adulthood, they can be remodeled to enhance plasticity through processes such as local release of ECM proteinases and microglia-mediated phagocytosis (34,38–40). Our findings indicate that Flx influences ECM organization pathways in mature granule cells, including upregulation of ECM proteinases like *Adamts6* and downregulation of core ECM components like *Tnr*, which encodes Tenascin-R (**Fig. 2A-B**).

To investigate whether ECM structures suppress developmental-like plasticity in the hippocampus, we first examined the ECM landscape. Using the lectin *wisteria floribunda agglutinin* (WFA), which binds ECM glycoproteins, we identified WFA-expressing PNNs and an abundance of non-PNN structures (**Fig. 4A**). While PNNs are well-studied, other ECM structures in the brain remain poorly understood. WFA levels were highest in CA2 and notably elevated in the DG hilus, which is densely occupied by mossy fiber terminals (**Fig. 4B**). In the hilus, WFA formed net-like structures reminiscent of PNNs, which we refer to as "perisynaptic nets" to distinguish them from PNNs (**Fig. 4C**). The holes in these nets were occupied by ZNT3+ mossy fiber terminals, suggesting a role in shaping the synaptic microenvironment (**Fig. 4D**). Perisynaptic nets were sparse in juvenile mice compared to adults, and 3 weeks of Flx treatment reduced their density in adulthood, potentially sculpting synaptic microenvironments more supportive of plasticity (**Fig. 4E-H**). Consistent with the slow timescale of ECM remodeling (41,42), no change in net density was observed after 5 days of Flx treatment. These findings reveal that chronic Flx treatment can remodel diffuse ECM structures, distinct from PNNs, in the DG.

Given that chronic Flx reduced peri-synaptic ECM and activated a developmental-like plasticity program in the DG, we investigated whether directly remodeling the ECM could restore this plasticity. While intracranial delivery of the bacterial enzyme Chondroitinase ABC (ChABC) is commonly used to degrade ECM proteoglycans, its effects lack spatial specificity and are transient due to ECM regeneration. To overcome these limitations, we injected an AAV encoding Cre-dependent expression of ChABC into the DG of Dock10-Cre mice, enabling cell-specific and constitutive secretion of ChABC from dentate granule cells (38; **Fig. 4I-J**). In Cort-treated mice, removal of ECM around granule cells was sufficient to reactivate SOX11 in granule cells (**Fig. 4K-M**). This data suggests that the ECM directly represses features of developmental plasticity.

We next tested if directly remodeling ECM in the DG was sufficient to produce antidepressant-like responses. In the EPM, we did not observe a significant difference in open arm exploration between Cort-treated ChABC and control mice (**Fig. 4N**). We observed a trend towards decreased latency to feed in ChABC mice in the NSF test, although this was not statistically significant (**Fig. 4O**). In the contextual fear generalization task, Cort-treated mice injected with control virus were unable to distinguish between the conditioned context A and unconditioned context B at day 14, indicating fear memory generalization overtime (**Fig. 4P-Q**). In contrast, Cort-treated mice injected with ChABC virus successfully distinguished between contexts A and B at day 14, suggesting that ECM removal can reduce stress-related fear generalization. Altogether, these results suggest that ECM remodeling is sufficient to mitigate stress-induced fear memory generalization.

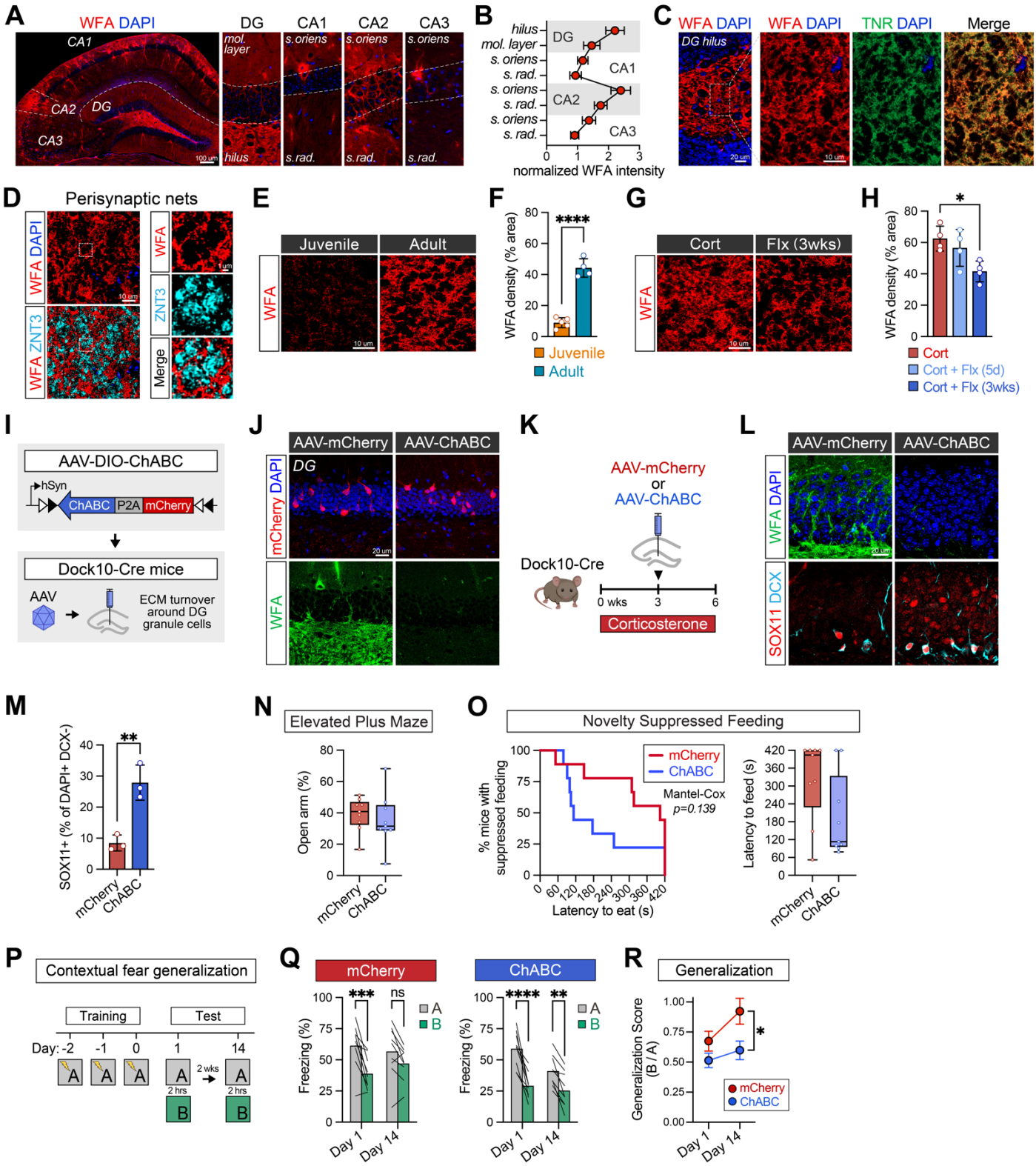

Figure 4. Turnover of extracellular matrix induces developmental-like plasticity and mitigates stress-induced fear memory generalization. (**A**) Representative image of WFA labeling in the hippocampus. (**B**) Quantification of WFA intensity in hippocampal subregions. (**C**) WFA labeling in the DG forms net-like structures ("perisynaptic nets") that are immunopositive for Tenascin-R (TNR). (**D**) Holes in perisynaptic nets are filled with ZNT3+ mossy fiber terminals; inset with higher magnification (right). (**E**) WFA staining in the DG hilus of juvenile (P10) and adult (~P120) mice. (**F**) Quantification of WFA levels in DG hilus per mouse (t-test, n= 5 (juvenile), 4 (adult)). (**G**) WFA staining in the DG hilus of adult mice treated with Cort or Cort + Flx (3wks). (**H**) Quantification of WFA levels in DG hilus per mouse (One-way ANOVA, Tukey's multiple comparisons test, n=4 mice/group). (**I**) Schematic of AAV-based strategy for cre-dependent expression of Chondroitinase ABC (ChABC) in dentate granule

cells. (**J**) Representative image of WFA levels around DG granule cells in mice injected with AAV-mCherry or AAV-ChABC. (**K**) Schematic for Cort treatment and AAV-ChABC delivery approach. (**L**) SOX11 expression in dentate granule cells in mice injected with AAV-mCherry or AAV-ChABC. DCX marks immature granule cells. (**M**) Quantification of SOX11+ granule cells per mouse (t-test, n= 3 (AAV-mCherry), 3 (AAV-ChABC)). (**N**) Time spent in the open arm of the EPM per mouse (t-test, n=9 mice (AAV-mCherry), 9 (AAV-ChABC). (**O**) Latency to feed in NSF per mouse injected with AAV-mCherry or AAV-ChABC shown as survival curve (left; Log-rank Mantel-Cox test, $\chi 2=2.19$, $p=0.139$) and box plot (right; Mann–Whitney U test, $p=0.124$, n= 9 mice/group). (**P**) Schematic of contextual fear generalization assay. (**Q**) Freezing in the fear conditioned context A versus unconditioned context B at 1 and 14 days post-training for mice injected with AAV-mCherry or AAV-ChABC (Two-way repeated measures ANOVA, Sidak's post hoc tests, n=9 mice/group). Lines connect paired data for each mouse. (**R**) Generalization scores at 1 and 14 days calculated as the freezing time in context B divided by context A (Two-way repeated measures ANOVA, Tukey's multiple comparisons tests). Data = mean ± SD. *$p < 0.05$; **$p < 0.01$; ***$p < 0.001$; ****$p < 0.0001$.

Discussion

Our study elucidates a novel mechanism underlying the effects of Flx on stress-related behaviors. Specifically, we demonstrate that Flx treatment remodels the ECM in the DG, reactivating a developmental-like plasticity program in mature granule cells. This ECM remodeling facilitates changes in neuronal plasticity possibly by loosening structural constraints and allowing enhanced synaptic remodeling. Such plasticity could be integral for resilience to the effects of chronic stress, with implications for reducing maladaptive generalization of negative memories. Our work highlights a critical molecular pathway through which an antidepressant exerts its behavioral effects and uncovers a novel modality for plasticity in the adult brain.

Methods

Animal studies

All mouse strains were maintained in the New York State Psychiatric Institute specific pathogen-free facility and maintained on a 12-hour light/dark schedule. Mouse protocols were approved by the Institutional Animal Care and Use Committee of Columbia University and the Research Foundation for Mental Hygiene, Inc. and were conducted in accordance with the NIH Guide for the Care and Use of Laboratory Mice. Care was taken to minimize the number of mice used and their suffering.

Littermate controls were used for all experiments when feasible, and all mice were backcrossed > 10 generations on a C57BL/6 background. Male mice were used throughout the manuscript except where otherwise noted.

Pharmacological approach

Corticosterone (Sigma, C2505) was dissolved at a concentration of 35 µg/mL in autoclaved deionized water containing 2 mg/mL beta-cyclodextrin (Chem-Impex, 32075) to improve solubility. The solution was then incubated in a 37°C water bath sonicator for 30 minutes to ensure complete dissolution. Fluoxetine hydrochloride (TCI Chemicals, F0750) was added at a final concentration of 160 ug/mL under the same conditions. Drug solutions were delivered ad libitum in drinking water in opaque bottles to protect from light. Fluoxetine concentrations were previously optimized to achieve brain pharmacokinetics equivalent to 18 mk/kg/day (44).

Behavioral assays

Conditioned fear was elicited by administering a 2 second footshock (0.75 mA) following a five-minute exposure to an array of contextual cues (conditioning chamber, chamber lights, white noise, scent of anise extract). Retrieval of the fear memory was assessed by a three-minute re-exposure of the animal to the conditioning context in the absence of shock where freezing (the cessation of all movement outside of respiration) was interpreted as expression of fear memory. Video recordings were acquired and scored automatically in FreezeFrame (Actimetrics). Mice were habituated to transport and holding in a separate room for at least one hour prior to all conditioning or retrieval sessions and subjected to three days of handling prior to all behavioral tests. For assessment of fear discrimination, freezing was measured in a context similar to the conditioning context two hours later, but with the following variations: the chamber fan was turned off, the scent

of lemon extract was used instead of anise, and a plastic divider was inserted to make the chamber walls circular and opaque. Freezing in the unconditioned context was tested two hours following retrieval testing in the original conditioning context, and animals were rested in a holding room between sessions. Freezing was scored

Anxiety-like behaviors were assessed via ten-minute exposure to the elevated plus maze (EPM) and seven-minute exposure to the novelty suppressed feeding (NSF) arena. Video recordings were acquired using Logitech webcams and OBS Studio software. Time spent in the open arms of the EPM were scored through automated object detection with the open-source ezTrack pipeline (45) and interpreted as anxiety-like behavior. Latency to feed in the NSF, defined as the amount of time a mouse took to first bite the food pellet, was manually scored using video recordings and live observation. Freezing and anxiety-like behaviors were both scored via an automated, unbiased process unless otherwise noted and all behavioral testing and analysis was performed blinded to treatment condition.

Single nuclei RNA sequencing

Intact hippocampi were isolated under a dissecting microscope and mechanically dissociated using a 2 mL glass tissue homogenizer (Kontes Glassware) on ice using twelve strokes of the tight pestle in 1% BSA-PBS. Nuclei were filtered using a 40 um strainer and then pelleted at 300 g for 5 minutes at 4°C. Nuclei were then resuspended in 22% Percoll (GE Healthcare) and centrifuged at 900 g for 20 minutes with acceleration set to 4 and deceleration set to 1 to remove cellular debris. The supernatant was removed and nuclei were washed with 1% BSA-PBS before being pelleted at 300 g for 5 minutes at 4°C and resuspended in 1% BSA-PBS to remove excess Percoll. All buffers contained Protector RNase Inhibitor (Roche) at 0.2 U/uL.

Hippocampal nuclei were sequenced using the 10x Single Cell Gene Expression 3' (v3) platform. Approximately 15,000 intact nuclei from each sample were loaded into each well of Chromium Chip A according to the manufacturer instructions and combined into droplets with barcoded beads using the Chromium controller. Libraries were prepared by the Single Cell Analysis Core of the Columbia University Sulzberger Genome Center following manufacturer instructions. The samples were sequenced to an average depth of 40,000-60,000 reads on an Illumina Novaseq 6000 sequencer.

Sequenced samples were processed using the Cell Ranger 6.1.2 pipeline and aligned to the mm10-2020-A mouse reference genome. Clustering and differential expression analysis were conducted in R v4.3.0 using Seurat v4.4.0 (46). Cells with fewer than 1,200 or over 3,600 detected genes/cell, or more than 5% mitochondrial DNA were excluded during quality control steps before identification of variable genes in the dataset, cell centering, and scaling. Additionally, genes that were expressed by fewer than 5 cells in the dataset were eliminated.

Immunohistochemistry and confocal microscopy

For all immunohistochemistry experiments, mice were transcardially perfused with ~10 mL of ice-cold 1X PBS followed by ~10 mL of 4% (weight/volume) paraformaldehyde diluted in PBS. Brains were post-fixed in 4% PFA for a minimum of 4 hours and then transferred to a 30% sucrose solution for a minimum of 2 days. Brains were then flash frozen and sliced in 40 um thick coronal sections on a HM 450 freezing microtome (Epredia).

For immunohistochemistry, brain sections were incubated in a blocking solution consisting of 10% normal goat or donkey serum (Thermo Fisher) and 0.4% Triton (Sigma-Aldrich) diluted in 1X PBS. Primary antibodies were diluted in 3% normal goat or donkey serum in 0.4% Triton and tissue was incubated on a shaker overnight at 4°C. Secondary antibodies were diluted in 3% normal goat or donkey serum and tissue was incubated on a shaker for 2 hours at room temperature with DAPI (Thermo Fisher) added at 1:5000 during the last 5 minutes of incubation. Brain sections were mounted on coverslips with ProLong Glass without DAPI (Thermo Fisher) for high resolution imaging and ProLong Gold (Thermo Fisher) for all other experiments.

For BDNF (Proteintech, 28205-1-AP) immunostaining, antigen retrieval was performed with IHC-Tek Epitope Retrieval Solution (IHC World), and brain sections were heated to 95°C for 40 minutes before washed 3x with PBS prior to blocking. Antigen retrieval for SOX11 (Sigma, MABE1929) and PROX1 (R&D Systems, AF2727) immunostaining was performed with the same procedure, but with a 10 minute incubation instead.

Histology slides were imaged on a Zeiss LSM 800 scanning confocal microscopes with Airyscan super-resolution module using a 63x objective for high resolution imaging and 20x objective for all other imaging experiments.

References

1. World Health Organization. Depression and Other Common Mental Disorders. In 2017 [cited 2025 Jan 2]. Available from: https://www.who.int/publications/i/item/depression-global-health-estimates

2. Nestler EJ, Barrot M, DiLeone RJ, Eisch AJ, Gold SJ, Monteggia LM. Neurobiology of depression. Neuron. 2002 Mar 28;34(1):13–25.

3. Santarelli L, Saxe M, Gross C, Surget A, Battaglia F, Dulawa S, et al. Requirement of Hippocampal Neurogenesis for the Behavioral Effects of Antidepressants. Science. 2003 Aug 8;301(5634):805–9.

4. Samuels BA, Anacker C, Hu A, Levinstein MR, Pickenhagen A, Tsetsenis T, et al. 5-HT1A receptors on mature dentate gyrus granule cells are critical for the antidepressant response. Nature Neuroscience. 2015 Nov 1;18(11):1606–16.

5. McEwen BS, Magarinos AM. Stress and hippocampal plasticity: implications for the pathophysiology of affective disorders. Hum Psychopharmacol. 2001 Jan;16(S1):S7–19.

6. David DJ, Samuels BA, Rainer Q, Wang JW, Marsteller D, Mendez I, et al. Neurogenesis-Dependent and -Independent Effects of Fluoxetine in an Animal Model of Anxiety/Depression. Neuron. 2009 May 28;62(4):479–93.

7. LeMoult J, Gotlib IH. Depression: A cognitive perspective. Clin Psychol Rev. 2019 Apr;69:51–66.

8. Leal SL, Tighe SK, Jones CK, Yassa MA. Pattern Separation of Emotional Information in Hippocampal Dentate and CA3. Hippocampus. 2014 Sep;24(9):1146–55.

9. Anacker C, Hen R. Adult hippocampal neurogenesis and cognitive flexibility - linking memory and mood. Nat Rev Neurosci. 2017 Jun;18(6):335–46.

10. Zhou Y, Su Y, Li S, Kennedy BC, Zhang DY, Bond AM, et al. Molecular landscapes of human hippocampal immature neurons across lifespan. Nature. 2022 Jul;607(7919):527–33.

11. Malberg JE, Eisch AJ, Nestler EJ, Duman RS. Chronic Antidepressant Treatment Increases Neurogenesis in Adult Rat Hippocampus. Journal of Neuroscience [Internet]. 2000 [cited 2017 Aug 14];20(24). Available from: http://www.jneurosci.org/content/20/24/9104?ijkey=b0678ce23159697a43bfec2545c4cff116cef6a4&keytype2=tf_ipsecsha

12. Duan Y, Wang SH, Song J, Mironova Y, Ming G li, Kolodkin AL, et al. Semaphorin 5A inhibits synaptogenesis in early postnatal- and adult-born hippocampal dentate granule cells. Elife. 2014 Oct 14;3:e04390.

13. Guo N, Soden ME, Herber C, Kim MT, Besnard A, Lin P, et al. Dentate granule cell recruitment of feedforward inhibition governs engram maintenance and remote memory generalization. Nature medicine. 2018 May;24(4):438–49.

14. Yonan JM, Steward O. Vector-mediated PTEN deletion in the adult dentate gyrus initiates new growth of granule cell bodies and dendrites and expansion of mossy fiber terminal fields that continues for months. Neurobiol Dis. 2023 Aug;184:106190.

15. Rayan NA, Kumar V, Aow J, Rastegar N, Lim MGL, O'Toole N, et al. Integrative multi-omics landscape of fluoxetine action across 27 brain regions reveals global increase in energy metabolism and region-specific chromatin remodelling. Mol Psychiatry. 2022 Nov;27(11):4510–25.

16. Samuels BA, Leonardo ED, Dranovsky A, Williams A, Wong E, Nesbitt AMI, et al. Global state measures of the dentate gyrus gene expression system predict antidepressant-sensitive behaviors. PLoS One. 2014;9(1):e85136.

17. Hensch TK. Critical period regulation. Annu Rev Neurosci. 2004;27:549–79.

18. Maya Vetencourt JF, Sale A, Viegi A, Baroncelli L, De Pasquale R, O'Leary OF, et al. The antidepressant fluoxetine restores plasticity in the adult visual cortex. Science. 2008 Apr 18;320(5874):385–8.

19. Karpova NN, Pickenhagen A, Lindholm J, Tiraboschi E, Kulesskaya N, Ágústsdóttir A, et al. Fear Erasure in Mice Requires Synergy Between Antidepressant Drugs and Extinction Training. Science. 2011 Dec 23;334(6063):1731–4.

20. Li Y, He X, Kawaguchi R, Zhang Y, Wang Q, Monavarfeshani A, et al. Microglia-organized scar-free spinal cord repair in neonatal mice. Nature. 2020 Nov;587(7835):613–8.

21. Scali M, Begenisic T, Mainardi M, Milanese M, Bonifacino T, Bonanno G, et al. Fluoxetine treatment promotes functional recovery in a rat model of cervical spinal cord injury. Sci Rep. 2013;3:2217.

22. Hochgerner H, Zeisel A, Lönnerberg P, Linnarsson S. Conserved properties of dentate gyrus neurogenesis across postnatal development revealed by single-cell RNA sequencing. Nature Neuroscience. 2018 Feb 15;21(2):290–9.

23. Esposito MS, Piatti VC, Laplagne DA, Morgenstern NA, Ferrari CC, Pitossi FJ, et al. Neuronal Differentiation in the Adult Hippocampus Recapitulates Embryonic Development. Journal of Neuroscience. 2005 Nov 2;25(44):10074–86.

24. Rasetto NB, Giacomini D, Berardino AA, Waichman TV, Beckel MS, Di Bella DJ, et al. Transcriptional dynamics orchestrating the development and integration of neurons born in the adult hippocampus. Sci Adv. 10(29):eadp6039.

25. Matson KJE, Russ DE, Kathe C, Hua I, Maric D, Ding Y, et al. Single cell atlas of spinal cord injury in mice reveals a pro-regenerative signature in spinocerebellar neurons. Nat Commun. 2022 Sep 26;13(1):5628.

26. Poplawski GHD, Kawaguchi R, Van Niekerk E, Lu P, Mehta N, Canete P, et al. Injured adult neurons regress to an embryonic transcriptional growth state. Nature. 2020 May;581(7806):77–82.

27. Norsworthy MW, Bei F, Kawaguchi R, Wang Q, Tran NM, Li Y, et al. Sox11 Expression Promotes Regeneration of Some Retinal Ganglion Cell Types but Kills Others. Neuron. 2017 Jun 21;94(6):1112-1120.e4.

28. Miao Q, Hill MC, Chen F, Mo Q, Ku AT, Ramos C, et al. SOX11 and SOX4 drive the reactivation of an embryonic gene program during murine wound repair. Nat Commun. 2019 Sep 6;10(1):4042.

29. Ramnauth AD, Tippani M, Divecha HR, Papariello AR, Miller RA, Nelson ED, et al. Spatiotemporal analysis of gene expression in the human dentate gyrus reveals age-associated changes in cellular maturation and neuroinflammation. bioRxiv. 2024 May 6;2023.11.20.567883.

30. Cohen-Cory S, Kidane AH, Shirkey NJ, Marshak S. Brain-derived neurotrophic factor and the development of structural neuronal connectivity. Dev Neurobiol. 2010 Apr;70(5):271–88.

31. Bath KG, Lee FS. Variant BDNF (Val66Met) impact on brain structure and function. Cogn Affect Behav Neurosci. 2006 Mar;6(1):79–85.

32. Erwin SR, Sun W, Copeland M, Lindo S, Spruston N, Cembrowski MS. A Sparse, Spatially Biased Subtype of Mature Granule Cell Dominates Recruitment in Hippocampal-Associated Behaviors. Cell Reports. 2020 Apr 28;31(4):107551.

33. Acsády L, Kamondi A, Sík A, Freund T, Buzsáki G. GABAergic cells are the major postsynaptic targets of mossy fibers in the rat hippocampus. J Neurosci. 1998 May 1;18(9):3386–403.

34. Frischknecht R, Gundelfinger ED. The brain's extracellular matrix and its role in synaptic plasticity. Adv Exp Med Biol. 2012;970:153–71.

35. Pizzorusso T, Medini P, Berardi N, Chierzi S, Fawcett JW, Maffei L. Reactivation of ocular dominance plasticity in the adult visual cortex. Science. 2002 Nov 8;298(5596):1248–51.

36. Gogolla N, Caroni P, Lüthi A, Herry C. Perineuronal nets protect fear memories from erasure. Science. 2009 Sep 4;325(5945):1258–61.

37. Moon LD, Asher RA, Rhodes KE, Fawcett JW. Regeneration of CNS axons back to their target following treatment of adult rat brain with chondroitinase ABC. Nat Neurosci. 2001 May;4(5):465–6.

38. Orlando C, Ster J, Gerber U, Fawcett JW, Raineteau O. Perisynaptic chondroitin sulfate proteoglycans restrict structural plasticity in an integrin-dependent manner. Journal of Neuroscience. 2012 Dec 12;32(50):18009–17.

39. Oray S, Majewska A, Sur M. Dendritic spine dynamics are regulated by monocular deprivation and extracellular matrix degradation. Neuron. 2004 Dec 16;44(6):1021–30.

40. Nguyen PT, Dorman LC, Pan S, Vainchtein ID, Han RT, Nakao-Inoue H, et al. Microglial Remodeling of the Extracellular Matrix Promotes Synapse Plasticity. Cell. 2020 Jul 23;182(2):388-403.e15.

41. Heo S, Diering GH, Na CH, Nirujogi RS, Bachman JL, Pandey A, et al. Identification of long-lived synaptic proteins by proteomic analysis of synaptosome protein turnover. Proc Natl Acad Sci U S A. 2018 Apr 17;115(16):E3827–36.

42. Tsien RY. Very long-term memories may be stored in the pattern of holes in the perineuronal net. Proc Natl Acad Sci U S A. 2013 Jul 23;110(30):12456–61.

43. Carstens KE, Gloss BR, Alexander GM, Dudek SM. Modified adeno-associated virus targets the bacterial enzyme chondroitinase ABC to select mouse neuronal populations in vivo using the Cre-LoxP system. Eur J Neurosci. 2021 Jun;53(12):4005–15.

44. Dulawa SC, Holick KA, Gundersen B, Hen R. Effects of chronic fluoxetine in animal models of anxiety and depression. Neuropsychopharmacology. 2004 Jul;29(7):1321–30.

45. Pennington ZT, Dong Z, Feng Y, Vetere LM, Page-Harley L, Shuman T, et al. ezTrack: An open-source video analysis pipeline for the investigation of animal behavior. Sci Rep. 2019 Dec 27;9(1):19979.

46. Stuart T, Butler A, Hoffman P, Hafemeister C, Papalexi E, Mauck WM, et al. Comprehensive Integration of Single-Cell Data. Cell. 2019 Jun 13;177(7):1888-1902.e21.